Hydrogenation of CO2 to Methanol by Pt Nanoparticles Encapsulated in UiO-67: Deciphering the Role of the MOF

Journal:	*Journal of the American Chemical Society*
Manuscript ID	Draft
Manuscript Type:	Article
Date Submitted by the Author:	n/a
Complete List of Authors:	Gutterød, Emil; Uinversity of Oslo, Department of chemistry Lazzarini, Andrea; Universitetet i Oslo, Chemistry Department Fjermestad, Torstein; Universitetet i Oslo, Chemistry Department Kaur, Gurpreet; Universitetet i Oslo, Chemistry Department Manzoli, Maela; University of Turin, Drug Science and Technology Bordiga, Silvia; Universita degli Studi di Torino, Department of Chemistry Svelle, Stian; Universitetet i Oslo, Department of Chemistry Lillerud, Karl; Uinversity of Oslo, Department of chemistry Skulason, Egill; Raunvisindastofnun Haskolans, Øien-Ødegaard, Sigurd; Universitetet i Oslo, Chemistry Department Nova, Ainara; Universitetet i Oslo, Centre for Theoretical and Computational Chemistry, Department of Chemistry Olsbye, Unni; Universitetet i Oslo, Chemistry;

Hydrogenation of CO_2 to Methanol by Pt Nanoparticles Encapsulated in UiO-67: Deciphering the Role of the MOF

Emil S. Gutterød[a], Andrea Lazzarini[a], Torstein Fjermestad[b], Gurpreet Kaur[a], Maela Manzoli[c], Silvia Bordiga[a,d], Stian Svelle[a], Karl P. Lillerud[a], Egill Skúlason[e], Sigurd Øien-Ødegaard[a], Ainara Nova[b], Unni Olsbye[a]*

[a]Centre for Materials Science and Nanotechnology, Department of Chemistry, University of Oslo, Sem Saelandsvei 26, N-0315 Oslo, Norway

[b]Hylleraas Centre for Quantum Molecular Sciences, Department of Chemistry, University of Oslo, P.O. Box 1033, Blindern, N-0315 Oslo, Norway

[c]Department of Drug Science and Technology and NIS - Centre for Nanostructured Interfaces and Surfaces, University of Turin, Via P. Giuria 9, Turin 10125, Italy

[d]Department of Chemistry, NIS Interdepartmental Centre and INSRM reference centre, University of Turin, via Quarello 15A, I-10135 Turin, Italy

[e]Science Institute and Faculty of Industrial Engineering, Mechanical Engineering and Computer Science, University of Iceland, VR-III, 107 Reykjavik, Iceland

Abstract

Metal-organic frameworks (MOFs) show great prospect as catalysts and catalyst support materials. Yet, studies that address their dynamic, kinetic and mechanistic role in target reactions are scarce. In this study, an exceptionally stable MOF catalyst consisting of Pt nanoparticles (NPs) embedded in a Zr-based UiO-67 MOF was subject to steady-state and transient kinetic studies involving H/D and $^{12}C/^{13}C$ exchange, coupled with operando infrared

spectroscopy and density functional theory (DFT) modeling, targeting methanol formation from CO_2/H_2 feeds at 170 °C and 1-8 bar pressure. The study revealed that methanol is formed at the interface between the Pt NPs and defect Zr nodes, via formate species attached to the Zr nodes. Methanol formation is mechanistically separated from the formation of co-products CO and methane, except for hydrogen activation on the Pt NPs. Careful analysis of transient data revealed that the number of formate intermediates was higher than the number of open Zr sites in the MOF lattice around each Pt NP. Hence, additional Zr sites must be available to formate formation. DFT modelling revealed that Pt NP growth is sufficiently energetically favored to enable displacement of linkers and creation of open Zr sites during pretreatment. However, linker displacement during formate formation is energetically disfavored, in line with the excellent catalyst stability observed experimentally. Overall, the study provides firm evidence that methanol is formed at the interface of Pt NPs and linker-deficient Zr_6O_8 nodes resting on the Pt NP surface.

Keywords: CO_2 hydrogenation, methanol, formate, transient kinetic analysis, kinetic isotope effect, operando FTIR, DFT, MOF, UiO-67.

Introduction

Atmospheric levels of CO_2 have risen at an alarming rate since the first half of the 20th century following our continuous and increasing use of fossil fuels. Large cuts in CO_2 emissions can be made through utilization of greener alternatives of energy production such as solar and wind power; however, these energy sources suffer from lack of continuity in energy output and requires efficient methods for large scale energy storage in order to compete with fossil fuels.[1]

One of the solutions to this problem is production of easily stored liquid fuels with high volumetric and gravimetric energy density, such as methanol, from CO_2 and green hydrogen.[2] This allows for continued use of already existing infrastructure.[3] Substantial research efforts have already been dedicated to the topic of valorizing CO_2 through hydrogenation, mainly with focus on the reverse water-gas shift (RWGS) reaction, methanation and methanol production.[4-13]

The product distribution of CO_2 hydrogenation varies significantly with the nature of the catalyst and operating conditions.[7] Most prior studies show that Pt-based systems are highly selective for the RWGS reaction, with minor selectivity towards methane.[11, 14-19] In that respect, Kattel et al.[18] performed a computational study of CO_2 hydrogenation over Pt nanoparticles supported on SiO_2 and TiO_2. They concluded that a RWGS and CO hydrogenation path, forming CO and small amounts of methane, dominate over those materials. This finding is in agreement with experimental evidence of CO formation mainly via surface carbonates. [15, 16]

Surface formates are also observed in several studies of the RWGS[15, 16, 20, 21] and of WGS[22-24] reactions; however, the significance of such a pathway over Pt-based catalysts is debated. In this regard, Burch, Goguet and Meunier[23] conducted a critical analysis of the experimental evidence for and against a formate mechanism over highly active Pt and Au WGS catalysts. They argue that most published results do not provide definite evidence for or against a formate pathway for the WGS reaction, and in the cases where reliable data are available, it is at most a minor and slow reaction pathway.

Recent studies show that when supporting Pt on a methane producing Co-oxide catalyst, methanol selectivity is observable under favorable conditions of low temperature and elevated pressure.[25-27] Furthermore, one prior study[28] demonstrated selectivity towards

methanol over oxide-supported Pt where the supports alone are inactive in CO_2 hydrogenation: out of a set of catalysts producing mainly CO (> 91 %), Pt/ZrO_2 showed the highest CH_3OH selectivity, reaching 6 % at 200 °C and 10 atm pressure.

Over the Zr-MOFs UiO-66 and -67, functionalized with Cu and Cu/Zn, high methanol selectivity is ascribed to an important role of the Zr-MOF interface in the reaction. Rungtaweevoranit et al.[29] found XPS evidence of Zr reduction in the presence of Cu when studying Cu NPs deposited on UiO-66 as a model system for the encapsulated version of the catalyst (i.e. Cu in UiO-66). Similar findings from XPS on CuZn@UiO-67 samples with 100% bipyridine-type linkers treated with reaction gas showed indications of Zr(IV) reduction to Zr(III), argued as caused by H adsorption.[30] In combination with H_2- and CO_2-TPD results, the authors suggested participation of the Zr-cluster in the reaction by means of H-spillover from Cu and CO_2 adsorption on unsaturated Zr-sites. When the catalyst was prepared with regular UiO-67 (i.e. biphenyl-type linkers), both the CH_3OH selectivity and catalytic stability decreased. Although the CuZn@UiO-67 material showed substantial activity in methanol formation, notably, both the crystallinity and specific surface area of the MOF were severely reduced already by the deposition of copper. Thus, the material did not exhibit the well-defined MOF structure of UiO-67 during the subsequent experiments.[30]

In a previous contribution, we reported the CO_2 hydrogenation activity and selectivity of an exceptionally stable Pt Zr-MOF catalyst, UiO-67-Pt, at ambient pressure. This catalyst maintains its well-defined MOF structure even after long-term operation and is therefore well suited as a model system for studying the influence of the MOF framework on the reaction. In the current study, the focus is set on elucidating the role of the UiO-67 framework in CO_2 hydrogenation to methanol through a kinetic investigation. In addition to standard steady-state

kinetic measurements, we employ H/D- and $^{13}C/^{12}C$ SSITKA, and *operando* FT-IR measurements, methods scarcely employed in MOF catalysis literature. In combination with DFT calculations, this work reveals unprecedented insight in the Pt–Zr-MOF interplay that leads to methanol formation during conversion of CO_2/H_2 mixtures at 170 °C and 1–8 bar.

Experimental Details

Details of material preparation and standard characterization methods (N_2 adsorption, ^{1}H-NMR, TGA, TEM and CO-chemisorption) are provided in the SI.

Operando FT-IR spectroscopy was performed using a Bruker Vertex70 instrument equipped with a liquid nitrogen-cooled MCT detector. Each spectrum was collected by averaging 64 acquisition with a resolution of 2 cm^{-1}. The sample (pressed in a self-sustained pellet of approx. 4 mg) was mounted inside a low free-volume cell from AABSPEC (model #CXX), by which pressure, temperature and gas flow are controllable. Due to the low sample amount, the CO_2 conversion was too low to be determined reliably and parallel experiments under comparable conditions were performed with the focus on gas-phase analysis (vide infra) . The sample was activated at 350 °C (5 °C/min ramp) in 10 % H_2/He (10 ml/min) for 4 hours, and then cooled to 170 °C in 10 ml/min He. The sample was kept under CO_2 hydrogenation (CO_2/H_2 = 1/6, 10 ml/min) reaction conditions for two hours, before the H_2 flow was exchanged to D_2.

Catalytic testing was performed in a fixed-bed flow setup with a straight stainless steel reactor (7 mm I.D.) operated under 1–8 bar, where effluent species is analyzed with an on-line Q-MS (Pfeiffer) and GC-TCD-FID (Agilent). The MOF samples were reduced for 4 hours at 350°C (5 °C/min ramp) in 20 ml/(min•0.1g_{cat}) flow of 10 % H_2/Ar under ambient pressure. Following the activation procedure, the reactor was cooled to 240 °C in inert flow, then

operated for 4 hours reaching steady-state under a set of reference conditions (1/6/3 CO_2/H_2/inert, 20 ml/min, 200 mg, τ = 0.01 g_{cat}•min/ml and ambient pressure) before changing conditions. The pre-reduced commercial samples Pt/SiO_2 (abcr), Pt/Al_2O_3 (Chimet) and Pt/C (Chimet), were heated directly to 240 °C under reference conditions, which were maintained until steady state was reached. Dependent on the experimental aim, 0.05–0.2 g catalyst was tested for CO_2 hydrogenation in range: 5–25 % CO_2, 40–90 % H_2, T = 170 °C, p = 1–8 bar and contact time τ = 0.004–0.04 g_{cat}•min/ml. A given set of operating conditions was fixed until steady state was reached and for at least two hours. During kinetic studies, changes in reaction conditions were performed in a random sequence. Each 3–4 set of conditions were the reference conditions. They showed that the change in catalyst performance was negligible during the kinetic studies. As reported in ref.[17] a minor increase in the catalytic activity and change in selectivity is observed for UiO-67-Pt during long-term operation. The same procedure as described above was followed in the H/D exchange experiments but with D_2 instead of H_2. H/D SSITKA experiments were performed by operating the catalysts at steady state under reference conditions, then switching the feed (1/6/3 CO_2/H_2/inert) rapidly to another feed containing D_2 instead of H_2 (1/6/3 CO_2/D_2/inert) using an electronically controlled 4-port 2-way valve. Switches back and forth between the two feeds were performed in intervals of 8 hours. $^{12}CO_2/^{13}CO_2$ SSTIKA experiments were performed in the same manner. The m/z values traced for each specie in the respective experiments are tabulated in Table S.

Results and Discussion

The UiO-66 series of Zr-MOFs (UiO-66, -67, -68) consists of Zr_6O_8 nodes connected by dicarboxylate-terminated linkers. The ideal linker-to-node ratio is 6:1, but prior investigations showed that factors like synthesis conditions (type of modulator and concentration, temperature and crystallization time) and activation conditions may strongly affect this ratio,

leading to materials that are commonly referred to as having “missing cluster” or “missing linker” defects, respectively.[31-37] Missing linker defects may be capped by modulator, anions of the MOF precursor salts, solvent or OH^-/H_2O pairs.[33, 36, 38, 39]

The current study was carried out using UiO-67 with 90 % biphenyl-4,4’-dicarboxylic acid (BPDC) linkers and 10 % 2,2’-bipyridine-5,5’-dicarboxylic acid (BPYDC) linkers, hereafter called **UiO-67-Pt**. Prior studies have demonstrated that the bipyridine entity in BPYDC is the preferred anchoring site for Pt salts in this MOF.[17, 40-42] In the current study, ^{1}H NMR analysis of digested material showed that the as-synthesized MOF contained 11 BPYDC linkers, 13 benzoic acid and 2 formic acid ligands, respectively, per 100 BPDC linkers (Table S3). Furthermore, Thermo-Gravimetric Analysis (TGA) measurements indicated that the as-synthesized MOF had a linker-to-node ratio of 5, suggesting that, in addition to benzoic acid and formic acid, the material contained Cl^- or OH^-/H_2O pairs, adding up to an average of 4 out of 24 Zr coordination sites per Zr_6O_8 node that were not connected to a linker molecule (Table S3).

After wet impregnation with the Pt NP precursor, K_2PtCl_4, the BPYDC and benzoic acid contents of UiO-67-Pt decreased slightly, while the formic acid content increased to 4 per 100 BPDC linkers (Table S2). Activation in a reducing atmosphere (10 % H_2/Ar flow at 350 °C, 1 bar, 4 h) transformed the Pt precursor salt into the active catalytic entity for CO_2 hydrogenation, Pt NPs.[17, 40, 42] In the current case, Transmission Electron Microscopy (TEM) investigations after activation showed the presence of Pt NPs homogeneously dispersed within the MOF framework (Figure S5). The Pt NPs supported on UiO-67 have average diameter of 3.6 ± 0.7 nm (Figure S5), i.e. larger than the diameter of the tetrahedral (1.2 nm) and octahedral (2.3 nm) cavities of the UiO-67 structure. Most of the Pt NPs displayed spherical shape, however,

careful inspection revealed the presence of NPs with squared borders and irregular shape, possibly exposing well defined terraces, after activation and after reaction (Figure S5 and Figure S6). Such features can arise from strong Pt-support interaction, and indeed, limited broadening of the Pt NP size distribution was observed after prolonged testing (Figure S6). A schematic illustration of a 3.6 nm Pt particle embedded in an 8 unit cell-enclosed octahedral cavity, mimicking a representative Pt NP observed by TEM, is presented in Scheme 1.

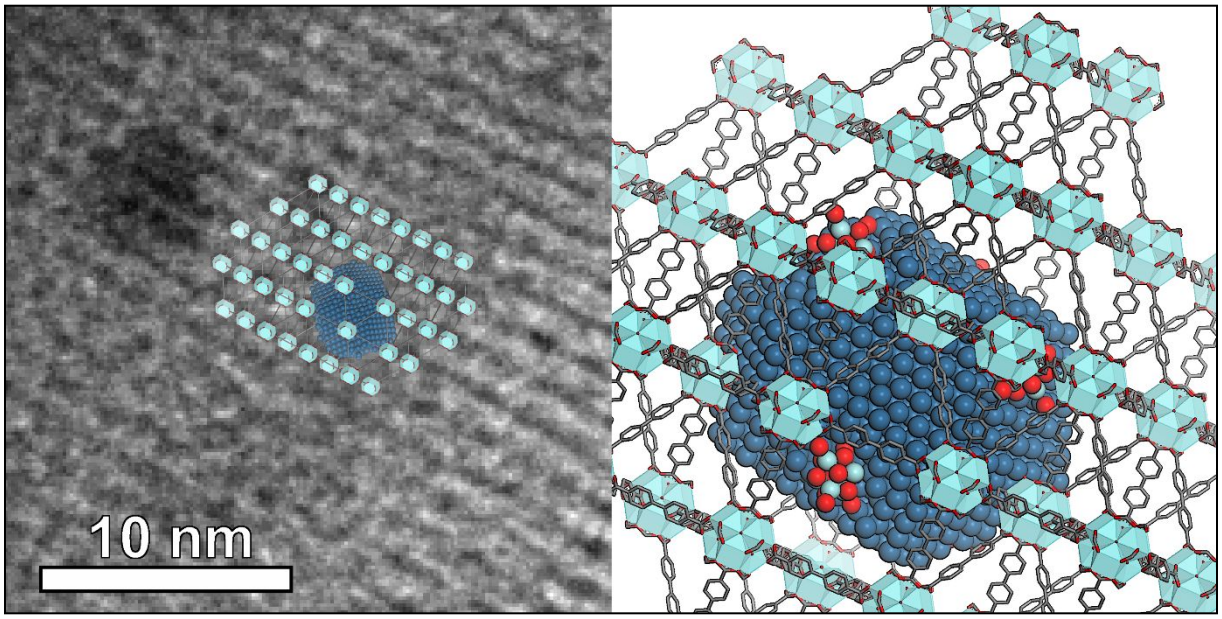

Scheme 1. Left: TEM micrograph showing the close packed (1 1 1) layers of Zr_6 clusters in UiO-67, with a spacing of 15.5 Å, overlaid with a 1600 atom Pt NP in the structure of UiO-67 viewed along (1 1 2) which is perpendicular to (1 1 1). Right: A 1600 atom Pt NP in UiO-67 viewed in the same direction. 6 Zr_6 clusters have been removed to accommodate the NP, and the ZrO_2 is decorating the NP surface.

CO_2/H_2 conversion and product selectivity obtained over Pt/C, Pt/SiO_2, Pt/Al_2O_3 and UiO-67-Pt at 170 °C and 1–8 bar is shown in Figure 1. Substantial selectivity differences were

observed at similar conversion levels (0.4–1.5 %): Over UiO-67-Pt, the methanol selectivity increased from around 3 to 19 %—corresponding to a turn-over-frequency (TOF) of 0.01 s^{-1}—when the pressure increased from 1 to 8 bar (Figure 1). This is, to the best of our knowledge, the second report of significant methanol formation from CO_2 over a Pt-based catalyst where the support alone is inactive in the reaction, and is the highest reported methanol selectivity and TOF over such a catalyst to date.[28] Under the same conditions, there was only a slight increase in methane selectivity from 1.2 to 1.6 %. Over Pt/Al_2O_3, both the methane and methanol selectivity reached 10 % under 8 bar pressure (Figure 1). In contrast to UiO-67-Pt, methane selectivity increased substantially with increasing pressure. Finally, over Pt/SiO_2 and Pt/C (Figure 1), CO was the only carbon-containing product observed, in accordance with the theory predictions of Kattel et al. for unsupported Pt NPs.[18] The formation of methanol over UiO-67-Pt points to strong metal-support interactions, as previously reported for Cu NPs embedded in UiO Zr-MOFs,[29, 30] and may suggest that the MOF support plays an active role during reaction, similarly to Al_2O_3 in the Water Gas Shift (WGS) and CO_2 hydrogenation reactions.[8, 24, 43]

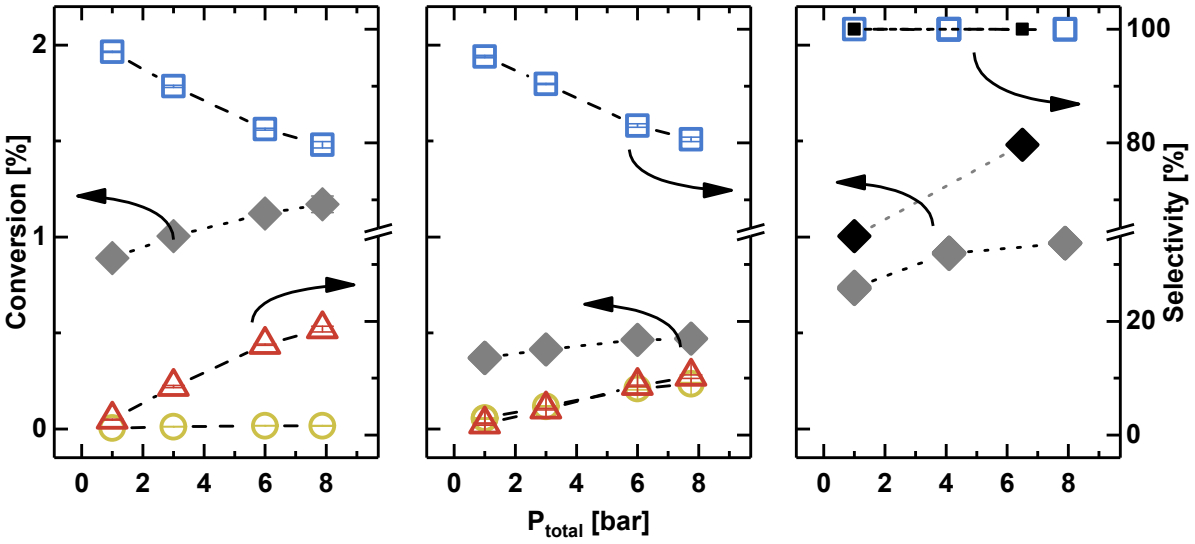

Figure 1. CO_2 conversion (left axes, diamonds) and product selectivity (right axes) during CO_2 hydrogenation under 1–8 bar total reaction pressure and T = 170 °C. Left: UiO-67-Pt. Middle: Pt/Al_2O_3. Right: Pt/SiO_2 (grey, red) and Pt/C (black). CO, CH_4 and CH_3OH selectivity is depicted as squares, circles and triangles, respectively. τ = 0.01 g_{cat}•min/ml, CO_2/H_2/inert = 1/6/3. For Pt/Al_2O_3 τ = 0.02 g_{cat}•min/ml.

To further assess the role of Pt NPs vs. support in CO_2 hydrogenation, steady-state H_2/D_2 exchange experiments were performed under CO_2 hydrogenation conditions over UiO-67-Pt, Pt/Al_2O_3, Pt/SiO_2, UiO-67 and SiO_2. The transient evolution of the HD molecule following a feed switch from $CO_2 + H_2$ to $CO_2 + D_2$ is shown in Figure S9. Importantly, formation of HD (and other products) was observed only over the Pt containing materials but not over the UiO-67 and SiO_2 supports alone, showing that dissociation of H_2/D_2 only occurs when Pt is present. The amount of HD formed over UiO-67-Pt and Pt/Al_2O_3 was larger than over Pt/SiO_2, and in all cases 1–2 orders of magnitude higher than the amount of exposed Pt atoms in Pt nanoparticles (Table 1). This observation, in combination with the observed HD tailing, strongly

suggests H/D exchange with hydroxyl groups on the support materials, either directly by hydrogen spillover to/from the Pt NPs, or by H/D exchange with the water molecules formed during reaction.

Table 1. Pt amount, NP diameter (d_{NP}), CO-uptake ($N_{A,CO,RT}$), estimated exposed Pt surface ($N_{surf,Pt}$) and the amount of HD formed ($N_{A,HD}$) after switching from H_2+CO_2 to D_2+CO_2 at 170 °C, 1 bar.

Catalyst	Pt amount (wt %)	d_{NP} (nm)	$N_{A,CO,RT}$ [c] ($\mu mol/g_{cat}$)	$N_{surf,Pt}$ [d] ($\mu mol/g_{cat}$)	$N_{A,HD}$ ($\mu mol/g_{cat}$)
UiO-67-Pt	2.7[a]	3.6 ± 0.7	1.7± 0.3	55	1200
Pt/Al_2O_3	5[b]	1.4[b]	36	200	1100
Pt/SiO_2	5[b]	5 ± 2	13	76	540
Pt/C	5[b]	2[b]	-	-	-

[a]theoretical amount of impregnation. [b]obtained from the provider. [c]pulse-chemisorption at room temperature. [d]estimated from TEM by following the procedure described in the SI.

Insights into the origin of HD tailing and formed amount over the UiO-67-Pt sample were obtained by a parallel *operando* FT-IR experiment under comparable conditions (1 bar, 170 °C, CO_2/H_2 = 1/6). When exchanging H_2 for D_2, the sharp signal of Zr-μ_3-OH at 3669 cm^{-1} [33] decreased to zero with time while another equally sharp and intense peak, corresponding to the deuterated species Zr-μ_3-OD, increased at 2705 cm^{-1} (Figure S16). Interestingly, quantification of the molar number of H in HD, $N_{A,HD}$, yields 1200 μmol H per gram catalyst, which corresponds to about 70 % of the theoretical number of Zr-μ_3-OH groups in the sample.

No other indication of H/D exchange (neither on Pt nor in linkers) was found from FT-IR experiments. More detailed description of the spectra obtained during FT-IR experiments over UiO-67-Pt, including the hydroxyl group region and the C-H bonds present in the aromatic linkers (carboxylates region is omitted as out of scale), is given in the supporting section (Figure S16). It is important to note that the chemical integrity of the catalyst is preserved during reaction and changes in the spectra are therefore caused by reaction products interacting with the sample. The most evident change is caused by the progressive increase of CO on the Pt nanoparticles (Figure 2). The shape and frequency of this signal is compatible with carbonyls linearly adsorbed on Pt atoms at the surface of NPs, as we already addressed in our previous study on an analogous material.[17] The size of the particles (3.6 nm) and the temperature (170 °C) justify the absence of bridged carbonyl species at lower frequencies. Changes in one of the smaller peaks in the IR spectra is the most novel observation of this study: the peak arising at 2745 cm^{-1} (Figure 2) is due to the appearance of formate groups (which, notably, are absent after activation, see Figure 2) most likely coming from the progressive process of CO_2 reduction. The frequency of this weak feature is compatible with the one of formates directly connected to open Zr-sites of the Zr-nodes in the MOF framework.[33, 44, 45] This is to the best of our knowledge, the first report of formate formation at the MOF Zr-node under CO_2 hydrogenation reaction conditions.

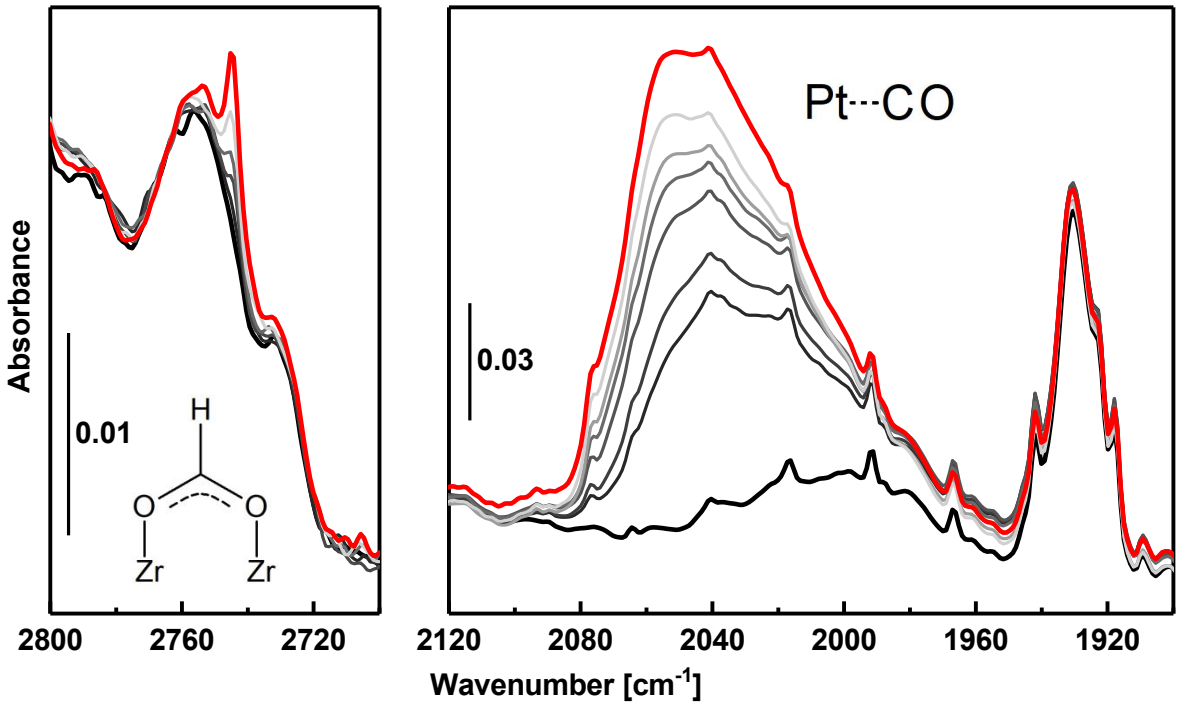

Figure 2. FT-IR spectra of UiO-67-Pt collected during CO_2 hydrogenation (CO_2/H_2 = 1/6, 10 ml/min, 170 °C, 1 bar) at different times (thick black curve for t = 0 min, grey scale from darkest to brightest for 0 < t < 120 min, thick red curve for t = 120 min). The left figure shows the magnified spectral region of the ν(C-H) for formate groups, while the right figure depicts the spectral interval typical for CO linearly adsorbed on metal nanoparticles. Full range spectra are reported in Figure S16.

The importance of this moiety is even more evident, thanks to the isotopic exchange experiment between H_2 and D_2. When exchanging H_2 for D_2 the signal of the ν(C-H) of the formate groups shifted from 2745 cm^{-1} to 2168 cm^{-1} [33] (Figure S16) and the intensity vastly increased as compared to the H-analogue ($I_{HCOO}/I_{DCOO} \approx 0.02$). The intensity increase indicates an inverse kinetic isotope effect, although possible differences in the extinction coefficient of the two species cannot be excluded. Importantly, a corresponding, gradual increase in methanol production rate was observed upon H_2/D_2 exchange under steady-state CO_2 hydrogenation conditions (Figure S14). At isotope equilibration, this difference in H- and D-

methanol production rates corresponds to an inverse Kinetic Isotope Effect (KIE) of 0.36. Moreover, the temporal scale of exchange was very similar for the formate species and for methanol in the parallel H_2/D_2 exchange experiments performed in the FT-IR transmission cell and the test-setup, respectively (Figure 3) (See Experimental section for details). Together, these experiments provide firm evidence that the Zr-formate species is a key intermediate in the methanol formation path.

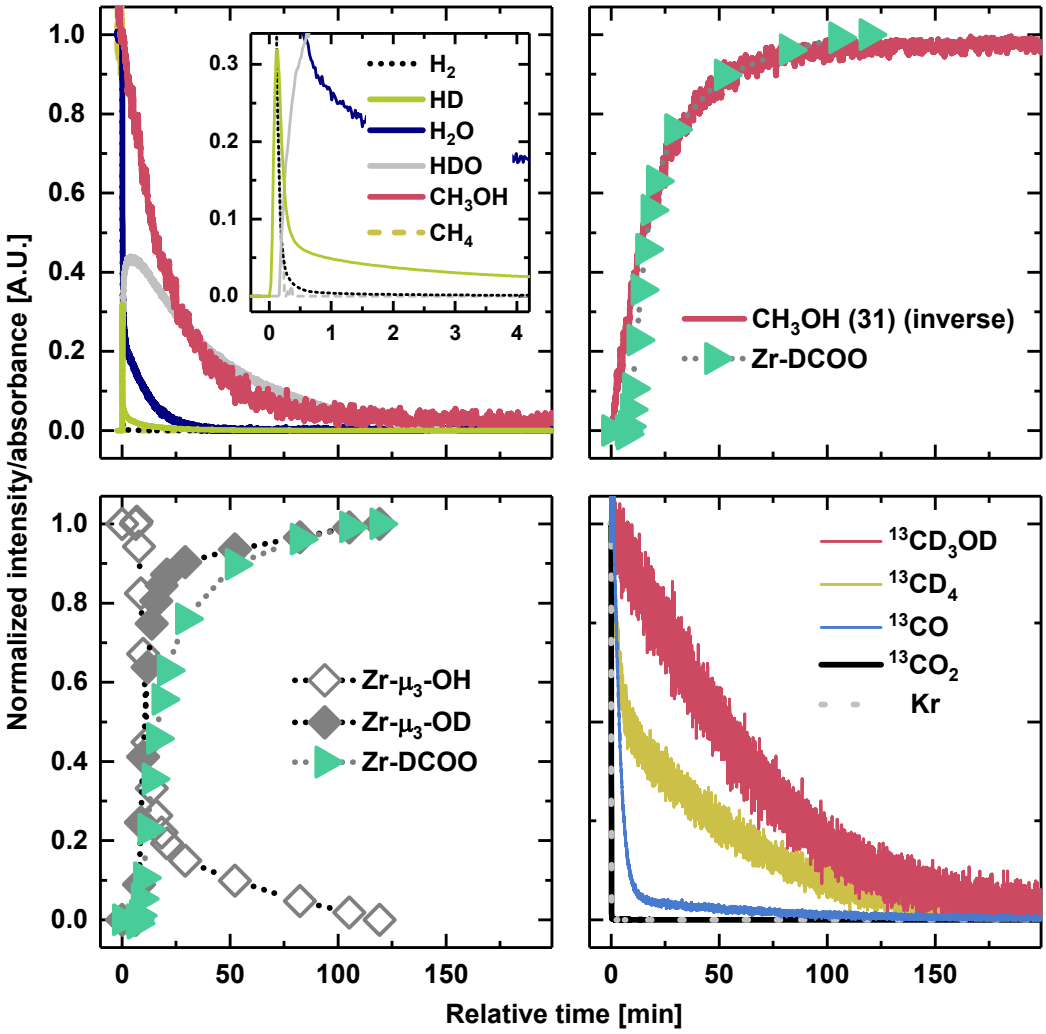

Figure 3. Top left: The normalized intensity of H_2 (m/z = 2), HD (m/z = 3), H_2O (m/z = 18), HDO (m/z = 19), CH_3OH (m/z = 31) and CH_4 (m/z =15) when switching from CO_2+H_2 to CO_2+D_2 at t = 0. Top right: Comparison of Zr-DCOO and CH_3OH (inverse) during H/D exchange. The

inset is a magnification of the first 4 minutes after the switch. Bottom left: Normalized absorbance of Zr-μOH (open diamonds), Zr-μOD (filled diamonds) and deuterated formate (triangles) during exchange of H_2 to D_2 at steady state CO_2 hydrogenation. $CO_2/H_2(D_2)$ = 1/6, 10 ml/min, 170 °C, 1 bar. Bottom right: The normalized intensity of Kr (m/z = 84), $^{13}CO_2$ (m/z = 45), ^{13}CO (m/z = 29), $^{13}CD_4$ (m/z = 21) and $^{13}CD_3OD$ (m/z = 35) products when switching from $^{13}CO_2 + D_2$ to $^{12}CO_2 + D_2$ at t = 0. T = 170 °C, 1bar, τ = 0.01 g_{cat}•min/ml.

Furthermore, during a complementary $(^{13}CO_2+D_2)/(^{12}CO_2+D_2)$ exchange experiment (Figure 3), $^{13}CD_3OD$ decreased steadily to zero in about 200 minutes, similarly to what observed for formate and methanol during the H_2/D_2 switch (Figure 3). The slope of the normalized intensity of methanol in a semi logarithmic plot (Figure S15) is inversely proportional to the mean surface residence time ($-1/\tau_{res}$) of intermediates leading to the formation of methanol (Table 3), and is characteristic of formation from a single pool of intermediates.[46]

Overall, the transient experiments provide firm evidence that formate species, attached to the Zr nodes in a bidentate configuration, are formed by H transfer from an adjacent Pt NP. Moreover, they strongly suggest that formate species are the most abundant surface intermediate to methanol formation, and hence, that hydrogenation of the formate species is the rate limiting step of methanol formation in UiO-67-Pt. Previously, an inverse KIE (albeit not as strong as in our case) was reported for CO_2 to methanol over $Cu/ZnO/Al_2O_3$, Cu/SiO_2, Cu/MgO and Pd/SiO_2.[10] In that case, DFT calculations predicted an inverse KIE for hydrogenation of the formate species, in line with our results.

Integration of the $^{13}C/^{12}C$ transient response of methanol showed an intermediate species concentration of 24 μmol/g (Table 3), i.e. close to half the amount of Pt surface species

estimated for the ensemble of Pt NPs identified by TEM (3.6 nm average diameter, Table 1). The schematic illustration of such a particle embedded in the MOF structure suggests that the average Pt NP contains 640 surface Pt sites, and is surrounded by 34 Zr nodes that have a total of 168 Zr-sites accessible for coordination at the Pt – MOF interface, corresponding to 84 bidentate formate species (Scheme 1, Figure 2). These numbers yield a formate:Pt surface site ratio of 84:640 (0.13), substantially lower than the estimated 24:55 (0.44) ratio from transient experiments.

Importantly, the numbers imply that additional Zr-sites are available to formate formation around each Pt NP. In this respect, we hypothesized that Zr-sites might become accessible by breaking Zr-linker bonds, either during Pt NP formation, or during the catalytic reaction. The hypotheses were investigated by periodic Density Functional Theory (DFT) calculations. (See SI for computational details and model construction). A Pt_{89} NP occupying the tetrahedral cavity of UiO-67 (Figure S17), $\mathbf{Pt_{89}^{tet}}$, was found to be an adequate model, justified by the assumption that the interface between the Pt NP and the linker/Zr node is similar when the NP has a diameter of 3.6 nm or ≈ 1 nm.

In the perfect MOF structure, all 24 coordination sites of each Zr-node are occupied by the carboxylate groups of the linker molecules. We first investigated the opening of such sites and computed the free energy profile of the system when a linker decoordinates from the node and slides along the Pt NP surface (Figure 4 and Figure S21). These calculations showed that it is unfavorable to open two Zr-sites ($\Delta G(\mathbf{Pt_{89}^{tet}} \rightarrow \mathbf{Pt_{89}^{tet}\text{-}II}$) = 16 kJ/mol), while opening one Zr-site is favorable, $\Delta G(\mathbf{Pt_{89}^{tet}} \rightarrow \mathbf{Pt_{89}^{tet}\text{-}I}$) = -54 kJ/mol). Considering next the catalytic reaction, the first step of formate formation is the adsorption of a CO_2 molecule which was found to coordinate its C atom to the Pt surface and the O atom to the opened Zr-site ($\Delta G_{ads}(\mathbf{Pt_{89}^{tet}\text{-}I}$ +

CO_2→ **CO_2*** = -20 kJ/mol) (Figure 4). Continuing on the formate formation pathway from the **CO_2*** intermediate, the two subsequent intermediates, **CO_2*+2H*** , ΔG(**Pt_{89}^{tet} + CO_2 +H_2 → CO_2*+2H***) = -144 kJ/mol and **HCO*O+H***, ΔG(**Pt_{89}^{tet} + CO_2 +H_2→HCO*O+H***) = -107 kJ/mol, correspond to H_2 adsorption on the Pt NP and a formate + hydride species, respectively (Figure 4). The H_2 adsorption is exergonic by -70 kJ/mol, and the subsequent H transfer to the C atom of CO_2 is endergonic by 37 kJ/mol. Interestingly, the transformation from **HCO*O+H*** to **HCO_2*+H***, ΔG(**Pt_{89}^{tet} + CO_2 +H_2→ HCO_2*+H***) = -29 kJ/mol, where the formate species is coordinated to two Zr-sites is highly endergonic, ΔG_r(**HCO*O+H*** → **HCO_2*+H***) = 78 kJ/mol. During the transformation from **HCO*O+H*** to **HCO_2*+H***, the linker decoordinates from one Zr-site and the significant endergonicity of this transformation is caused by the displacement of the linker, as described above.

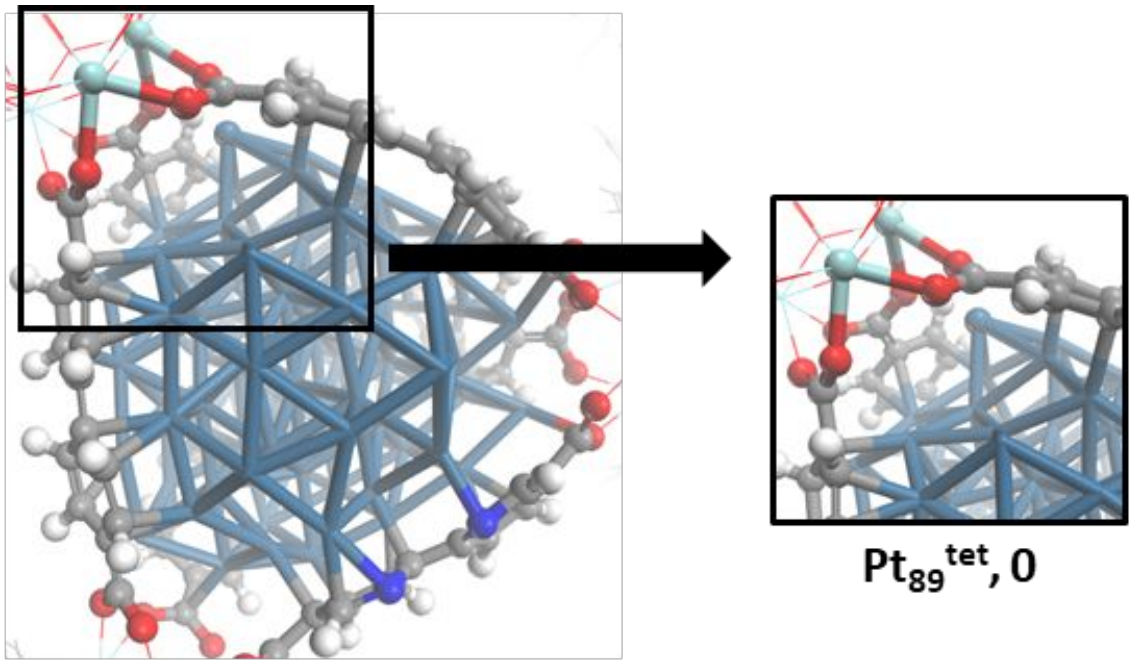

Pt_{89}^{tet}, 0

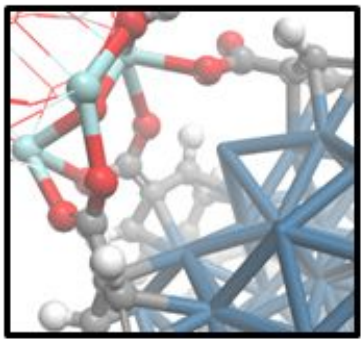

Pt_{89}^{tet}-I, -54

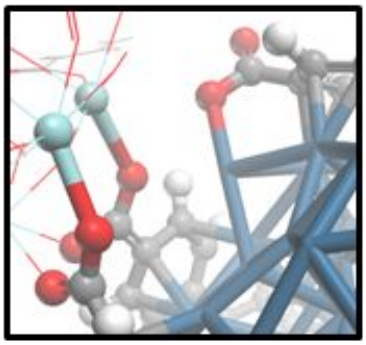

Pt_{89}^{tet}-II, -16

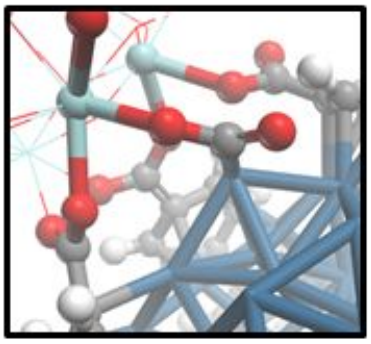

CO_2*, -74

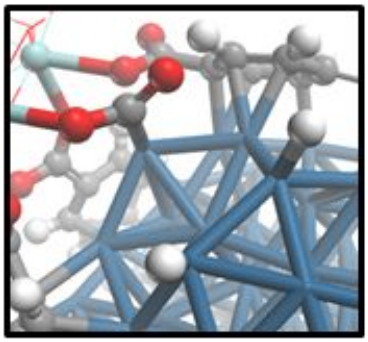

CO_2*+2H*, -144

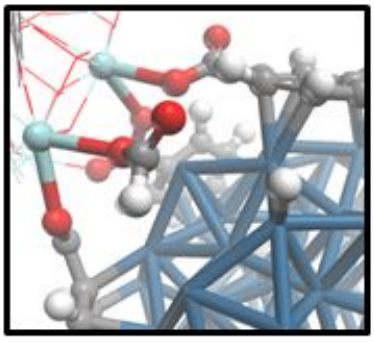

HCO*O+H*, -107

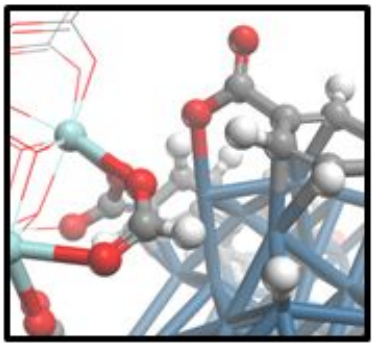

HCO_2*+H*, -29

Figure 4. 3D representations of intermediates of the reaction pathway towards the formation of the formate species coordinated to two Zr sites, HCO_2*+H*. Values are free energies in kJ/mol.

These results suggest that in order to generate a formate species coordinated to two Zr sites, a Zr node decoordinated from linkers must already be present. It was then explored whether the growth of the Pt NP during activation could cause the formation of such Zr nodes with open coordination sites. Insight into this possibility was obtained by computing the free energy of the Pt particle growth from Pt_{55}^{tet} to Pt_{89}^{tet}. These calculations showed that the reaction free energy of the system decreases as the Pt NP grows, and the decrease in energy will eventually exceed the energy loss of linker detachment (Figure S18 and Figure S19). Thus, during the nanoparticle growth, linkers will detach from the Zr nodes, and the Zr nodes will decorate the growing Pt nanoparticle. Returning to Scheme 1, the number of Zr nodes that needs to be removed from a perfect MOF lattice in order to create the 3.6 nm model Pt NP is between 6 and 13, depending on the orientation of the Pt NP. The corresponding number of additional bidentate formate sites is 72-156; the higher number being in line with the experimentally observed numbers.

Support for the computational results were found from on-line Mass Spectrometry (MS) measurements performed during activation in 10% H_2/Ar atmosphere at 350 °C. The MS data revealed traces of phenyl-containing fragments in the effluent gas, suggesting that modulator and/or linker molecules desorbed from the material during Pt NP formation (Figure S8). Further support for a partial degradation of the MOF framework around the Pt particles during activation was found from the specific surface area of the UiO-67-Pt material, which increased

slightly after activation and catalytic testing (Figure S). The crystallographic features of the material were unchanged (Figure S2, Figure S5 and Figure S6) and the BPYDC/BPDC ratio remained constant during subsequent testing (Table S2). Furthermore, no linker fragments were observed during a second activation of UiO-67-Pt after testing, in line with the excellent catalyst stability observed under reaction conditions.

Having established the importance of the Zr-nodes and formate intermediates for methanol formation over UiO-67-Pt, the next issue is whether methanol formation could be decoupled from CO and CH_4 formation, hence, optionally leading to higher methanol selectivity. To this end, we first turn to classical kinetic experiments.

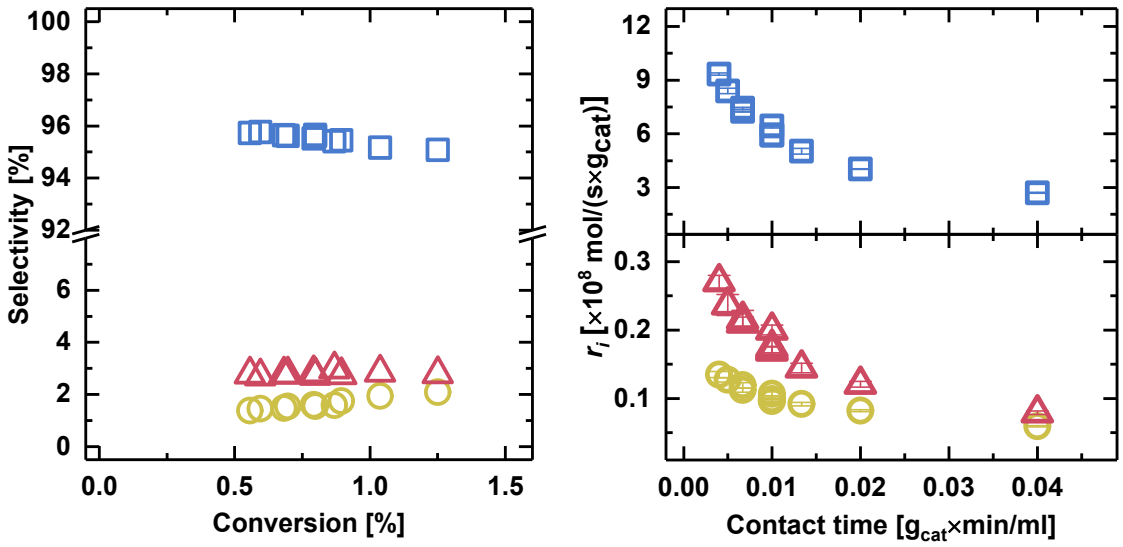

Figure 5. Contact time variation during CO_2 hydrogenation to CO (squares), CH_4 (circles) and CH_3OH (triangles) at 170 °C, 1 bar, $CO_2/H_2/He$ = 1/6/3 and τ = 0.004–0.04 g_{cat}•min/ml. Left: Selectivity versus conversion. Right: Rate of product formation versus contact time.

Contact time variation experiments, under otherwise constant conditions, showed that methanol selectivity is constant when CO_2 conversion increases, suggesting that it is a primary reaction product (Figure 5). Conversely, methane selectivity increases with increasing CO_2

conversion, while CO selectivity decreases, suggesting that CH_4 is mainly a secondary product, formed via CO. The latter result is in accordance with our previous studies of an analogous catalyst at higher temperature.[17]

Next, partial pressure variation experiments were performed in order to assess reaction orders for each product. This assessment was complicated by the decreased formation rate of all products with increasing contact time (Figure 5), indicating strong adsorption of one or several reaction products, thereby poisoning the active site(s).[10, 19] Indeed, when correlating the rate decrease with the partial pressures of the majority products, CO and H_2O, all products have a reaction order close to negative 1 in $p(CO+H_2O)$, CH_4 slightly less negative (Figure S10 and Table 2). Based on FT-IR results reported above, showing that CO adsorbed on Pt (2042 cm^{-1})[17] dominates the Pt surface under the respective reaction conditions, CO was assessed as the main contributor to the inhibition, likely suppressing the coverage in H[8] by competitive adsorption. When taking into account the variable concentration of CO and H_2O, positive reaction orders in pH_2 and pCO_2 were observed for all products, but with substantial differences (Table 2).

Considering first the majority product, CO, its formation rate depends strongly on $P(CO_2)$, but less on $p(H_2)$ (Table 2). Furthermore, no Kinetic Isotope Effect (KIE) was observed for CO during the $(CO_2+H_2)/(CO_2+D_2)$ transient experiment (Table S5 and Figure S14), showing that breaking or making of H-H or H-O bonds (which would otherwise lead to a primary KIE)[10, 47] is not rate-determining for CO formation under the conditions studied here. Finally, the number of surface intermediates leading to CO formation and their mean residence time were calculated from the $^{13}C/^{12}C$ transients (Table 3 and Figure 3). The normalized ^{13}CO signal rapidly decreased to around 0.05 within the first 15 minutes then

slowly reached zero in the following 150 minutes. It is interesting to note that the number of surface intermediates leading to CO formation represents 66% of the Pt surface atoms in Pt NPs, estimated from TEM measurements (Table 1 vs. Table 3). This observation, in combination with the partial coverage of the Pt NPs by Zr-nodes (and linkers), the inhibiting effect of CO, the high predicted barrier of CO desorption from Pt,[18] and the observation of a positive correlation between facile CO desorption and rate of CO formation in our previous study,[17] strongly suggest CO desorption as rate-limiting step in the RWGS reaction over UiO-67-Pt.

Table 2. Reaction orders in total pressure (p_{total}), and in pH_2, pCO_2 and $p(CO+H_2O)$ (1 bar) for the rate of conversion (X) and CO, CH_4 and CH_3OH formation at 170 °C over UiO-67-Pt.

p_i	X	CO	CH_4	CH_3OH
P_{total}	0.1	0	0.3	1.1
$CO+H_2O$[a]	-1.1	-1.1	-0.7	-1
H_2[b]	0.2	0.2	0.9	1.7
CO_2[b]	0.9	0.9	0.1	0.7

[a]Estimated from contact time variation experiments (Figure 5 and Figure S10). The reaction orders represent the average of two experiments. [b]Reaction orders when taking into account variable pCO and pH_2O in the reactor.

Turning next to methane formation rate, it depends strongly on $P(H_2)$ and weakly on $P(CO_2)$ (Table 2). Considering the high coverage of CO, as well as the presumed indirect formation of methane via CO, this result is not surprising. In the $(CO_2+H_2)/(CO_2 + D_2)$ transient experiment, an inverse KIE of 0.6, i.e. intermediate between CO (KIE = 1) and

methanol (KIE = 0.36), was observed for methane (Table S5 and Figure S14). Intriguingly, the inverse KIE was installed within the 15 minutes resolution of the gas analysis, hence, much more rapid than the transient behavior of methanol (Figure S14). Thus, the rate-determining step of methane formation involves bonding with hydrogen,[47-50] but the rate-determining step is not the same as for methanol formation. Indeed, the much more rapid transient behavior of methane compared to formate, disqualifies formate as a significant intermediate to methane formation. This result implies that, except for hydrogen activation, methane formation is mechanistically decoupled from methanol formation. The normalized CH_4 formation rate (represented by the m/z = 15 signal of CH_3) also decreases rapidly to zero (comparable to H_2) during the H/D exchange (Figure 3). Due to their mass overlap with the much more abundant water fragments, the time evolution of partially exchanged methane/methyl species could not be followed. The transient behavior of methane during the $^{13}C/^{12}C$ switch (Figure 3) was markedly different from that observed in the H/D transient: The normalized $^{13}CD_4$ formation rate decreased to 0.5 during the first 7 minutes and then slowly to zero in the following 160 minutes. This distinct shape of the isotope transient indicates methane formation from two pools in parallel,[46, 51] one rapidly converted to products and the other more slowly. Integration of the transient curve showed that the number of surface intermediates leading to methane formation is low (Table 3). Moreover, about 3 % of the methane-forming intermediates react fast and is responsible for about 50 % of the steady-state methane formation rate, while the other 97 % react slowly, with a semi-logarithmic evolution (Table 3 and Figure S15).

Returning finally to methanol, its formation depends strongly on both reactant partial pressures, in line with the observation that it is a primary product, formed independently of CO (Figure 5). The $^{13}C/^{12}C$ transient experiment shows that methanol is formed from a similar

number of surface intermediates as CO, but their turn-over rate is much slower, hence leading to the 9 % methanol selectivity observed under the respective conditions (Table 3).

Table 3. Mean surface residence times τ_{res} and the number N_{ad} of surface intermediates leading to the formation of ^{13}CO, $^{13}CD_4$ and $^{13}CD_3OD$ at 170 °C (1 bar), calculated from integration of the curves in Figure 3 and the isotope-independent steady-state reaction rates.

	INT(CO)	INT(CD_4)	INT(CD_3OD)
N_{ads} (μmol/g_{cat})	31	3.2	24
τ_{res} (s)	540	2174	3897

Considering finally the non-carbon products HD, H_2O and HDO, they exhibited slow or partially slow transient responses (Figure 3). HD has a sharp initial peak with considerable tailing over the course of the following hour, indicating formation from parallel pools and/or exchange with hydrogen-containing surface species.[52] H_2O showed transient characteristics suggestive of parallel pools, similar to CO and CH_4, and the HDO signal increased rapidly to a maximum within a few minutes then slowly decreased over the course of 2 hours, closely following the methanol signal. The long surface lifetime of these products is indicative of a long-lived source of H participating in their formation, presumably also in the formation of methanol. Interestingly, quantification of the mol H in HD, H_2O, HDO and CH_3OH yields 1500 μmol H per gram catalyst, which corresponds to about 80 % of the theoretical amount of mol Zr μ_3-OH groups in the sample (HD accounts for 70%, as reported above).

Conclusion

Mechanistic aspects of CO_2 hydrogenation over UiO-67-Pt and the role of the UiO-67 framework have been investigated in detail by employment of steady-state and transient kinetic studies, coupled with *operando* infrared spectroscopy and DFT modeling.

It was observed that Pt NPs embedded in the MOF structure are responsible for hydrogen activation, and that formate species are formed at the Zr nodes by reaction between adsorbed CO_2 and hydrogen spill-over from an adjacent Pt NP. These results demonstrate that the Pt NPs strongly interact with defect Zr nodes during reaction, and hence, that Zr nodes decorate the surface of the Pt NPs. Formate species are the most abundant intermediates in the reaction path to methanol, and transient results suggest that formate hydrogenation is the rate-limiting step of methanol formation. Importantly, the abundance of formate species is limited by the number of Zr sites made available by linker detachment due to Pt NP growth during catalyst activation. No evidence was found of further linker detachment during catalytic testing, nor during a second activation period after testing.

CO and methane formation are mechanistically separated from methanol formation, except for the hydrogen dissociation step. The main route to methane formation is proposed as CO hydrogenation. Moreover, the presented data are consistent with CO desorption being the rate limiting step of the reverse water gas shift reaction over UiO-67-Pt.

Acknowledgement

E.S.G, A.L., G.K., S.Ø.-Ø., S.B., S.S., K.P.L. and U.O. acknowledge the Research Council of Norway for financial support (FRINATEK ToppForsk Grant No. 250795 CONFINE). We further acknowledge Chimet for providing Pt/Al_2O_3 and Pt/C catalysts.

T.F. acknowledge the Norwegian Metacenter for Computational Science (NOTUR) for computational resources (projects number nn4654k and nn4683k), Michele Cacella for useful advice on the methodology, Sri Harsha Pulumati for fruitful discussions, Jingyun Ye and J. Karl Johnson for help with reproducing their calculations of reference [53].

T.F., E.S. and A.N. acknowledge support by the 'Nordic Consortium for CO2 Conversion' (NordForsk project No. 85378, site.uit.no/nordco2).

A. N. acknowledge the support from the Research Council of Norway (FRINATEK Grant No. 250044 and Center of Excellence Grant No. 262695).

Author Information

Corresponding Author

*unni.olsbye@kjemi.uio.no

Associated Content

Supporting Information

Catalyst preparation, characterization, catalytic testing, operando FTIR and computational details.

References

1. Bellotti, D.; Rivarolo, M.; Magistri, L.; Massardo, A. F. Feasibility study of methanol production plant from hydrogen and captured carbon dioxide. *J. CO2 Util.* **2017,** *21*, 132-138.

2. Chu, S.; Cui, Y.; Liu, N. The path towards sustainable energy. *Nat. Mater.* **2016,** *16*, 16.

3. Olah, G. A. Beyond Oil and Gas: The Methanol Economy. *Angew. Chem. Int. Ed* **2005,** *44* (18), 2636-2639.

4. Porosoff, M. D.; Yan, B.; Chen, J. G. Catalytic reduction of CO2 by H2 for synthesis of CO, methanol and hydrocarbons: challenges and opportunities. *Energy Environ. Sci.* **2016,** *9* (1), 62-73.

5. Wang, W.; Wang, S.; Ma, X.; Gong, J. Recent advances in catalytic hydrogenation of carbon dioxide. *Chem. Soc. Rev.* **2011,** *40* (7), 3703-3727.

6. Li, W.; Wang, H.; Jiang, X.; Zhu, J.; Liu, Z.; Guo, X.; Song, C. A short review of recent advances in CO2 hydrogenation to hydrocarbons over heterogeneous catalysts. *RSC Adv.* **2018,** *8* (14), 7651-7669.

7. Kattel, S.; Liu, P.; Chen, J. G. Tuning Selectivity of CO2 Hydrogenation Reactions at the Metal/Oxide Interface. *J. Am. Chem. Soc.* **2017,** *139* (29), 9739-9754.

8. Wang, X.; Shi, H.; Kwak, J. H.; Szanyi, J. Mechanism of CO2 Hydrogenation on Pd/Al2O3 Catalysts: Kinetics and Transient DRIFTS-MS Studies. *ACS Catal.* **2015,** *5* (11), 6337-6349.

9. Wu, H. C.; Chang, Y. C.; Wu, J. H.; Lin, J. H.; Lin, I. K.; Chen, C. S. Methanation of CO2 and reverse water gas shift reactions on Ni/SiO2 catalysts: the influence of particle size on selectivity and reaction pathway. *Catal. Sci. Technol.* **2015,** *5* (8), 4154-4163.

10. Kunkes, E. L.; Studt, F.; Abild-Pedersen, F.; Schlögl, R.; Behrens, M. Hydrogenation of CO2 to methanol and CO on Cu/ZnO/Al2O3: Is there a common intermediate or not? *J. Catal.* **2015,** *328*, 43-48.

11. Chen, X.; Su, X.; Duan, H.; Liang, B.; Huang, Y.; Zhang, T. Catalytic performance of the Pt/TiO2 catalysts in reverse water gas shift reaction: Controlled product selectivity and a mechanism study. *Catal. Today* **2017,** *281*, 312-318.

12. Hartadi, Y.; Widmann, D.; Behm, R. J. Methanol formation by CO2 hydrogenation on Au/ZnO catalysts – Effect of total pressure and influence of CO on the reaction characteristics. *J. Catal.* **2016,** *333*, 238-250.

13. Gaikwad, R.; Bansode, A.; Urakawa, A. High-pressure advantages in stoichiometric hydrogenation of carbon dioxide to methanol. *J. Catal.* **2016,** *343*, 127-132.

14. Román-Martínez, M. C.; Cazorla-Amorós, D.; Linares-Solano, A.; Salinas-Martínez de Lecea, C. CO2 hydrogenation under pressure on catalysts Pt□Ca/C. *Appl. Catal. A* **1996,** *134* (1), 159-167.

15. Kim, S. S.; Park, K. H.; Hong, S. C. A study of the selectivity of the reverse water–gas-shift reaction over Pt/TiO2 catalysts. *Fuel Process. Technol.* **2013,** *108*, 47-54.

16. Goguet, A.; Meunier, F. C.; Tibiletti, D.; Breen, J. P.; Burch, R. Spectrokinetic investigation of reverse water-gas-shift reaction intermediates over a Pt/CeO2 catalyst. *J. Phys. Chem. B* **2004,** *108* (52), 20240-20246.

17. Gutterød, E. S.; Øien-Ødegaard, S.; Bossers, K.; Nieuwelink, A.-E.; Manzoli, M.; Braglia, L.; Lazzarini, A.; Borfecchia, E.; Ahmadigoltapeh, S.; Bouchevreau, B.; Lønstad-Bleken, B. T.; Henry, R.; Lamberti, C.; Bordiga, S.; Weckhuysen, B. M.; Lillerud, K. P.; Olsbye, U. CO2 Hydrogenation over Pt-Containing UiO-67 Zr-MOFs—The Base Case. *Ind. Eng. Chem. Res.* **2017,** *56* (45), 13206-13218.

18. Kattel, S.; Yan, B.; Chen, J. G.; Liu, P. CO2 hydrogenation on Pt, Pt/SiO2 and Pt/TiO2: Importance of synergy between Pt and oxide support. *J. Catal.* **2016,** *343*, 115-126.

19. Kim, S. S.; Lee, H. H.; Hong, S. C. A study on the effect of support's reducibility on the reverse water-gas shift reaction over Pt catalysts. *Appl. Catal. A* **2012,** *423*, 100-107.

20. Tibiletti, D.; Goguet, A.; Meunier, F. C.; Breen, J. P.; Burch, R. On the importance of steady-state isotopic techniques for the investigation of the mechanism of the reverse water-gas-shift reaction. *Chem. Commun.* **2004,** (14), 1636-1637.

21. Jacobs, G.; Davis, B. H. Reverse water-gas shift reaction: steady state isotope switching study of the reverse water-gas shift reaction using in situ DRIFTS and a Pt/ceria catalyst. *Appl. Catal. A* **2005,** *284* (1), 31-38.

22. Kalamaras, C. M.; Panagiotopoulou, P.; Kondarides, D. I.; Efstathiou, A. M. Kinetic and mechanistic studies of the water–gas shift reaction on Pt/TiO2 catalyst. *J. Catal.* **2009,** *264* (2), 117-129.

23. Burch, R.; Goguet, A.; Meunier, F. C. A critical analysis of the experimental evidence for and against a formate mechanism for high activity water-gas shift catalysts. *Appl. Catal. A* **2011,** *409-410*, 3-12.

24. Kalamaras, C. M.; Olympiou, G. G.; Efstathiou, A. M. The water-gas shift reaction on Pt/γ-Al2O3 catalyst: Operando SSITKA-DRIFTS-mass spectroscopy studies. *Catal. Today* **2008,** *138* (3), 228-234.

25. Ouyang, B.; Xiong, S.; Zhang, Y.; Liu, B.; Li, J. The study of morphology effect of Pt/Co3O4 catalysts for higher alcohol synthesis from CO2 hydrogenation. *Appl. Catal. A* **2017,** *543*, 189-195.

26. Sápi, A.; Rajkumar, T.; Ábel, M.; Efremova, A.; Grósz, A.; Gyuris, A.; Ábrahámné, K. B.; Szenti, I.; Kiss, J.; Varga, T.; Kukovecz, Á.; Kónya, Z. Noble-metal-free and Pt nanoparticles-loaded, mesoporous oxides as efficient catalysts for CO2 hydrogenation and dry reforming with methane. *J. CO2 Util.* **2019,** *32*, 106-118.

27. Liu, B.; Ouyang, B.; Zhang, Y.; Lv, K.; Li, Q.; Ding, Y.; Li, J. Effects of mesoporous structure and Pt promoter on the activity of Co-based catalysts in low-temperature CO2 hydrogenation for higher alcohol synthesis. *J. Catal.* **2018,** *366*, 91-97.

28. Inoue, T.; Iizuka, T. Hydrogenation of carbon dioxide and carbon monoxide over supported platinum catalysts. *J. Chem. Soc. Faraday Trans. 1* **1986,** *82* (6), 1681-1686.

29. Rungtaweevoranit, B.; Baek, J.; Araujo, J. R.; Archanjo, B. S.; Choi, K. M.; Yaghi, O. M.; Somorjai, G. A. Copper Nanocrystals Encapsulated in Zr-based Metal–Organic Frameworks for Highly Selective CO2 Hydrogenation to Methanol. *Nano Lett.* **2016,** *16* (12), 7645-7649.

30. An, B.; Zhang, J.; Cheng, K.; Ji, P.; Wang, C.; Lin, W. Confinement of Ultrasmall Cu/ZnOx Nanoparticles in Metal–Organic Frameworks for Selective Methanol Synthesis from Catalytic Hydrogenation of CO2. *J. Am. Chem. Soc.* **2017,** *139* (10), 3834-3840.

31. Kaur, G.; Øien-Ødegaard, S.; Lazzarini, A.; Chavan, S. M.; Bordiga, S.; Lillerud, K. P.; Olsbye, U. Controlling the Synthesis of Metal–Organic Framework UiO-67 by Tuning Its Kinetic Driving Force. *Cryst. Growth Des.* **2019,** *19* (8), 4246-4251.

32. Wu, H.; Chua, Y. S.; Krungleviciute, V.; Tyagi, M.; Chen, P.; Yildirim, T.; Zhou, W. Unusual and Highly Tunable Missing-Linker Defects in Zirconium Metal–Organic Framework UiO-66 and Their Important Effects on Gas Adsorption. *J. Am. Chem. Soc.* **2013,** *135* (28), 10525-10532.

33. Yang, D.; Ortuño, M. A.; Bernales, V.; Cramer, C. J.; Gagliardi, L.; Gates, B. C. Structure and Dynamics of Zr6O8 Metal–Organic Framework Node Surfaces Probed with Ethanol Dehydration as a Catalytic Test Reaction. *J. Am. Chem. Soc.* **2018,** *140* (10), 3751-3759.

34. Shearer, G. C.; Chavan, S.; Bordiga, S.; Svelle, S.; Olsbye, U.; Lillerud, K. P. Defect Engineering: Tuning the Porosity and Composition of the Metal–Organic Framework UiO-66 via Modulated Synthesis. *Chem. Mater.* **2016,** *28* (11), 3749-3761.

35. Feng, L.; Yuan, S.; Zhang, L.-L.; Tan, K.; Li, J.-L.; Kirchon, A.; Liu, L.-M.; Zhang, P.; Han, Y.; Chabal, Y. J.; Zhou, H.-C. Creating Hierarchical Pores by Controlled Linker Thermolysis in Multivariate Metal–Organic Frameworks. *J. Am. Chem. Soc.* **2018,** *140* (6), 2363-2372.

36. Shearer, G. C.; Chavan, S.; Ethiraj, J.; Vitillo, J. G.; Svelle, S.; Olsbye, U.; Lamberti, C.; Bordiga, S.; Lillerud, K. P. Tuned to Perfection: Ironing Out the Defects in Metal–Organic Framework UiO-66. *Chem. Mater.* **2014,** *26* (14), 4068-4071.

37. Shearer, G. C.; Forselv, S.; Chavan, S.; Bordiga, S.; Mathisen, K.; Bjørgen, M.; Svelle, S.; Lillerud, K. P. In Situ Infrared Spectroscopic and Gravimetric Characterisation of the Solvent Removal and Dehydroxylation of the Metal Organic Frameworks UiO-66 and UiO-67. *Top. Catal.* **2013,** *56* (9), 770-782.

38. Trickett, C. A.; Gagnon, K. J.; Lee, S.; Gándara, F.; Bürgi, H.-B.; Yaghi, O. M. Definitive Molecular Level Characterization of Defects in UiO-66 Crystals. *Angew. Chem. Int. Ed* **2015,** *54* (38), 11162-11167.

39. Øien, S.; Wragg, D.; Reinsch, H.; Svelle, S.; Bordiga, S.; Lamberti, C.; Lillerud, K. P. Detailed Structure Analysis of Atomic Positions and Defects in Zirconium Metal–Organic Frameworks. *Cryst. Growth Des.* **2014,** *14* (11), 5370-5372.

40. Braglia, L.; Borfecchia, E.; Lomachenko, K. A.; Bugaev, A. L.; Guda, A. A.; Soldatov, A. V.; Bleken, B. T. L.; Oien, S.; Olsbye, U.; Lillerud, K. P.; Bordiga, S.; Agostini, G.; Manzoli, M.; Lamberti, C. Tuning Pt and Cu sites population inside functionalized UiO-67 MOF by controlling activation conditions. *Faraday Discuss.* **2017**.

41. Øien, S.; Agostini, G.; Svelle, S.; Borfecchia, E.; Lomachenko, K. A.; Mino, L.; Gallo, E.; Bordiga, S.; Olsbye, U.; Lillerud, K. P.; Lamberti, C. Probing Reactive Platinum Sites in UiO-67 Zirconium Metal–Organic Frameworks. *Chem. Mater.* **2015,** *27* (3), 1042-1056.

42. Braglia, L.; Borfecchia, E.; Martini, A.; Bugaev, A. L.; Soldatov, A. V.; Øien-Ødegaard, S.; Lønstad-Bleken, B. T.; Olsbye, U.; Lillerud, K. P.; Lomachenko, K. A.; Agostini, G.; Manzoli, M.; Lamberti, C. The duality of UiO-67-Pt MOFs: connecting treatment conditions and encapsulated Pt species by operando XAS. *Phys. Chem. Chem. Phys.* **2017,** *19* (40), 27489-27507.

43. Wang, X.; Shi, H.; Szanyi, J. Controlling selectivities in CO2 reduction through mechanistic understanding. *Nat. Commun.* **2017,** *8* (1), 513.

44. Busca, G.; Lamotte, J.; Lavalley, J. C.; Lorenzelli, V. FT-IR study of the adsorption and transformation of formaldehyde on oxide surfaces. *J. Am. Chem. Soc.* **1987,** *109* (17), 5197-5202.

45. Tibiletti, D.; Meunier, F. C.; Goguet, A.; Reid, D.; Burch, R.; Boaro, M.; Vicario, M.; Trovarelli, A. An investigation of possible mechanisms for the water–gas shift reaction over a ZrO2-supported Pt catalyst. *J. Catal.* **2006,** *244* (2), 183-191.

46. Ledesma, C.; Yang, J.; Chen, D.; Holmen, A. Recent Approaches in Mechanistic and Kinetic Studies of Catalytic Reactions Using SSITKA Technique. *ACS Catal.* **2014,** *4* (12), 4527-4547.

47. Ojeda, M.; Li, A.; Nabar, R.; Nilekar, A. U.; Mavrikakis, M.; Iglesia, E. Kinetically Relevant Steps and H2/D2 Isotope Effects in Fischer−Tropsch Synthesis on Fe and Co Catalysts. *J. Phys. Chem. C* **2010,** *114* (46), 19761-19770.

48. Watson, D. T. P.; Ge, Q.; King, D. A. Facile H–D exchange in adsorbed methylidyne on Pt{110}–(1×2) and deuteration to gaseous methane. *J. Chem. Phys.* **2001,** *115* (24), 11306-11316.

49. Polanyi, M. Reaction Rates of the Hydrogen Isotopes. *Nature* **1934,** *133*, 26.

50. Bawn, C. E. H.; Ogden, G. Wave mechanical effects and the reactivity of the hydrogen isotopes. *Trans. Faraday Soc.* **1934,** *30* (0), 432-443.

51. Shannon, S. L.; Goodwin, J. G. Characterization of Catalytic Surfaces by Isotopic-Transient Kinetics during Steady-State Reaction. *Chem. Rev.* **1995,** *95* (3), 677-695.

52. Xie, J.; Yang, J.; Dugulan, A. I.; Holmen, A.; Chen, D.; de Jong, K. P.; Louwerse, M. J. Size and Promoter Effects in Supported Iron Fischer–Tropsch Catalysts: Insights from Experiment and Theory. *ACS Catal.* **2016,** *6* (5), 3147-3157.

53. Ye, J.; Johnson, K. J. Design of Lewis Pair-Functionalized Metal Organic Frameworks for CO2 Hydrogenation. *ACS Catal.* **2015,** *5*, 2921-292

Graphical abstract